Key Engineering Materials
ISSN: 1662-9795, Vol. 1048, pp 51-61
doi:10.4028/p-vg6IX7

Submitted: 2025-12-19
Revised: 2026-02-16
Accepted: 2026-02-24
Online: 2026-04-14

Lightweight Battery Housings from Thin-Walled, Large-Scale Aluminum Profiles by Hot Extrusion

Oliver Schulz[1,a*], Sebastian Wurth[2,b], Alessandro Selvaggio[3,c], Johannes Gebhard[1,d], Yannis P. Korkolis[1,e], Patrik Bieker[2,f], Thomas Kloppenborg[2,g]

[1]Institute of Forming Technology and Lightweight Components (IUL), TU Dortmund University, Baroper Straße 303, 44227 Dortmund, Germany

[2]OTTO FUCHS KG, Derschlager Straße 26, 58540 Meinerzhagen, Germany

[3]ISPT GmbH & Co. KG, Carlo-Schmid-Allee 3, 44263 Dortmund, Germany

[a*]Oliver.Schulz@iul.tu-dortmund.de, [b]sebastian.wurth@otto-fuchs.com, [c]selvaggio@ispt-solutions.com, [d]johannes.gebhard@iul.tu-dortmund.de, [e]yannis.korkolis@iul.tu-dortmund.de, [f]patrik.bieker@otto-fuchs.com, [f]thomas.kloppenborg@otto-fuchs.com

Keywords: EV, FEM, die design, process control, size scaling

Abstract. The transition towards sustainable mobility demands lightweight and modular carrier systems for high-voltage batteries and fuel cells that combine structural efficiency with effective thermal management. This study examines the feasibility of producing thin-walled, large-scale aluminum extrusion profiles for modular battery housings using AA6063. Numerical simulations and experimental trials are conducted to optimize die design and define process limits along the relation between circumscribing circle diameter (*CCD)* and minimal wall thickness t_{min}. Furthermore, different quenching methods are used to investigate the influence on surface distortion and final mechanical properties. A streamlined die design with reduced mandrel deflection has enabled defect-free extrusion under controlled conditions for the extrusion of a thin-walled, large-scale profile with a *CCD*-to-t_{min} ratio of 138. A narrow process window is identified for extrusion of defect-free profiles. Quenching studies have shown that active cooling methods affect surface deformation but have negligible influence on mechanical properties or microstructure due to efficient heat extraction inherent to thin-wall geometries for the investigated alloy. Scaling experiments using an enlarged cross section by a factor of 2.5 have confirmed similar process stability without wall thickness adjustments, achieving up to 38 % weight reduction compared with conventional designs under industrial conditions.

Introduction

Modular carrier systems for high-voltage traction batteries and fuel cells must combine structural efficiency with minimal mass while ensuring thermal management capability within vehicle architectures. Current lightweight battery housing concepts predominantly utilize fluid-cooled aluminum extrusion profiles, assembled into compact enclosures due to their favorable strength-to-weight ratio and heat transfer properties [1]. To further improve stiffness-to-weight ratio and volumetric energy density of the overall system, recent developments aim at joining large-scale hollow profiles into extended panel-type load-bearing structures [2].

In this context, modularity has become a key design principle for next-generation battery housings. The ability to adapt joining strategies, such as friction-stir-welding or mechanical joining [3], enables flexible configuration of profile assemblies according to specific environmental demands. For instance, housings designed for passenger vehicles prioritize lightweight integration and contribution to body stiffness, whereas truck applications require enhanced robustness and scalability in size. Investigating these concepts allows tailoring mechanical performance, sealing integrity and manufacturability across diverse operating conditions.

The realization of thin-walled, large-format extrusions required for such modular battery housings is constrained by technological limitations along the process chain, often described by the relation between circumscribing circle diameter (*CCD)* and minimal wall thickness t_{min} [4]. Reduced wall thicknesses lead to higher mechanical loads on extrusion dies and increase sensitivity in subsequent joining and machining operations due to higher risk of distortion. Furthermore, scaling the profile geometry introduces several challenges to the extrusion process, ranging from die stability to quenching uniformity and distortion control.

However, systematic reduction of profile wall thickness combined with robust control of subsequent processing steps offers a substantial lightweight potential. Finite-element-based research on die design has already contributed to extending these limits allowing for *CCD*-to-t_{min} ratios of up to 170 [5]. In particular, the investigation of the die geometry continues to offer potential for weight reduction. By improving the material flow through adaption of the bridges and reducing mandrel deflection, thinner profile walls can be achieved and therefore a weight reduction of 16 % is possible [6].

In an alternative hot extrusion approach multiple smaller containers (and billets) next to each other and an adapted die geometry is used to extrude profiles [7]. Due to the die geometry the multiple material flows weld inside the die, comparable to a conventional porthole die. The reduction in friction area and ram force increases the extrudability of wide and thin-walled profiles [8]. Although this method offers a significant improvement regarding the limitations of conventional extrusion, new container and punches are required, limiting the adaption on existing presses.

Therefore, the investigation of the lightweight potential for the conventional extrusion process remains essential. Especially, comprehensive investigations into feasible process windows for thin-walled, large-scale profiles and overcoming the limitations by adjusting the die geometry offer great potential. Consequently, this paper focuses on the *CCD*-to-t_{min} ratio as a current limiting parameter for extrusion processes found in the industry and on extending it by die adaptation using the example of a battery housing. Furthermore, size scaling effects on both the extrusion and subsequently quenching processes are investigated to realize a modular battery carrier system tailored to the application.

Methods

Materials. For the investigations, the aluminum alloy AA6063 is selected due to its technological significance and economic relevance in extrusion applications, especially for the automotive sector. The material is cast in accordance to the European standard for wrought aluminum (EN AW) and supplied in billet diameters of 140 mm and 344 mm to be extruded on a 10 MN and a 55 MN extrusion press. The chemical composition is listed in **Table 1**.

Table 1. Chemical composition of the used aluminum alloy AA6063

Element	Si	Fe	Cu	Mn	Mg	Cr	Zn	Ti
Weight %	0.557	0.234	0.032	0.041	0.506	0.009	0.072	0.020

Battery Concept. To ensure the modularity of the battery housings, the available volume must be utilized as efficiently as possible. The biggest influence on the battery housing cross section is therefore the cell format used. These formats can be divided into the three main groups: cylindrical, prismatic and pouch cells [9]. Due to the rectangular shape of prismatic battery cells and their efficient thermal management [10] , this format, so called PHEV2, is chosen here as a relatively generic cell type. Based on this a hollow rectangular profile with two quadratic chambers is introduced (**Figure 1a**), which can be stacked modularly to fit different applications (**Figure 1b**). Due to the limits of the available extrusion press in the laboratory, a maximum *CCD* of 160 mm is determined. The measurements of the proposed cross section (**Figure 1c**) include a *CCD* of 160 mm with a wall thickness of t = 1 mm resulting in a *CCD*-to-t_{min} ratio of 160. As seen in the literature, such as [11], a minimal wall thickness of t_{min} = 2 mm would conventionally be necessary for this kind of *CCD*.

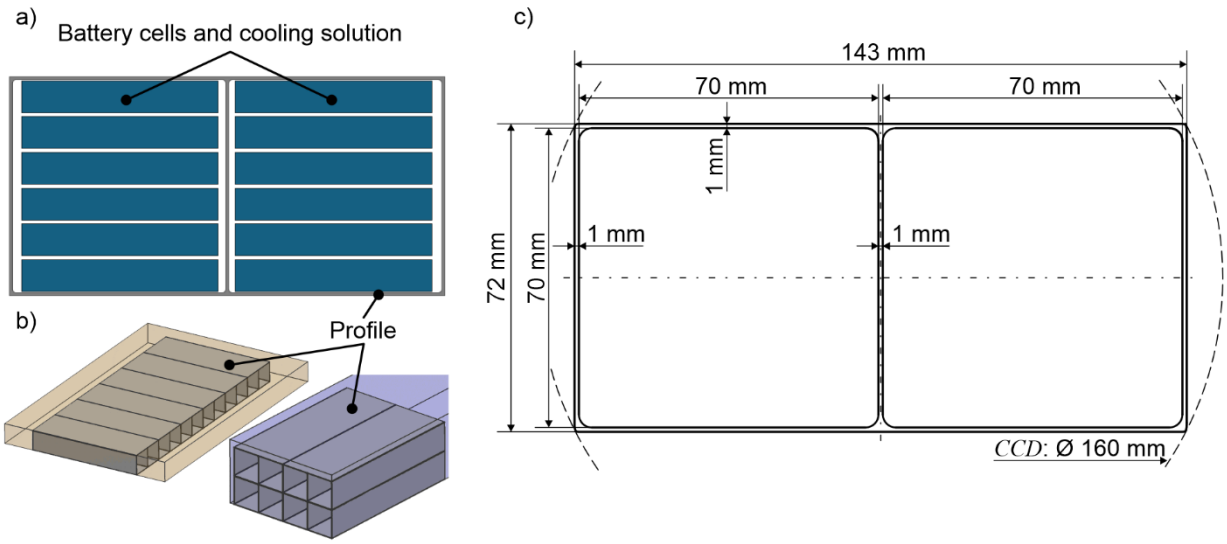

Fig. 1. a) Schematic of the battery housing architecture including battery cells and cooling solution, b) Modular profile stacking for different applications, c) initial proposed profile cross section for the battery housing for the laboratory scale.

To evaluate the modularity of the concept and to investigate size-scaling effects during extrusion and quenching, the initial cross section is enlarged by a factor of 2.5. The inner and outer radii, as well as chamfers, remain unchanged. This modification results in a more industrially representative profile size, corresponding to a typical battery housing used in electric vehicles. The geometrical quality of the profiles is defined and measured by their dimensional accuracy and mechanical properties according to DIN EN 755-9 and DIN EN 755-2 respectively.

Numerical investigation of the tool design. Before running extrusion trials, the tool design was investigated with the help of FEM simulations using Altair`s Inspire Extrude Metal. In the program, the steady state regime is modeled using the Eulerian approach on the basis of the flow volume generated from the tool model (**Figure 2a**). For the discretization of the model, around $2.5 \cdot 10^6$ first-order tetrahedral and prismatic elements are used. A minimum of 5 elements over the thickness in every area and an aspect ratio limit of 5 are ensured, fulfilling the recommendations for the solver. The plastic behavior of the material is modelled using the Zener and Hollomon model [12] modified by Sellars and Tegart [13] with parameters from the software's database for AA6063. Due to the different friction behaviors typically found in extrusion, two friction models are used. Sticking friction is assumed on the container and die wall, while Altair´s proprietary viscoplastic friction model ($\tau = f(P, \sigma_f, \mu)$) with a friction coefficient $\mu = 0.3$ is used in the bearing zone. The process model also accounts for the die deflection by automatically coupling the contact forces, generated from the calculated pressure in the flow volume, on to the tool surface. For modeling of the elasto-plastic tool behavior, the database's standard material model for tool steel H13 is used. The movement of the die and mandrel is restricted on the mantle surfaces and the surfaces connected to the bolster (**Figure 2b**). The contact between the die and mandrel part of the tool is defined as 'separating', to allow separation and movement of both parts individually. For the process parameters a typical parameter set for the laboratory press is used: $T_{Billet} = 550$ °C, $T_{Die} = 450$ °C and $v_{ram} = 2$ mm/s. The numerical model is finally validated using the force displacement curves and temperature measurements of the experiments, showing maximum deviation of 5% for the tool temperature and 7 % deviation of the force value.

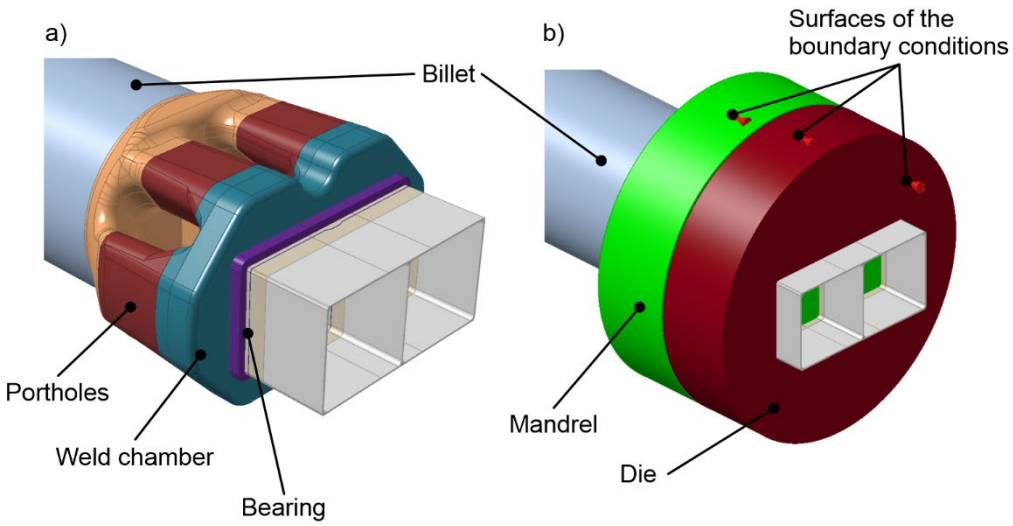

Fig. 2. Numerical setup of the extrusion process with tool deflection analysis: a) flow volume of the material inside the die and b) die setup with flow volume

Experimental setup. The extrusion trials are conducted on a 10 MN and a 55 MN extrusion press at the Institute of Forming Technology and Lightweight Components IUL and OTTO FUCHS KG, respectively. For the smaller scale, the initial container and die temperature of $T_{container} = T_{die} = 400$ °C is set through heating elements inside the machine frame, die and container. The billets are heated to $T_{billet} = 550$ °C in an external convection furnace. To achieve the steady state quicker and to reduce tool deflection during fill-up, three additional billets are extruded beforehand at $T_{billet} = 575$ °C to heat-up the die. In this way, the starting temperature for the first analyzed extrusion cycle is above 450 °C. The actual die temperature depends on the billet loading time. For the investigation of the temperature evolution during extrusion, a total of 6 thermocouples are integrated into the die with three being at the bearing edge and three at the weld chamber. An additional pyrometer is used to measure the surface temperature in the middle of the top surface at the die exit. Subsequently cooling of the profiles is realized with a quenching box [3], developed at the IUL (**Figure 3**), that enables three different types of cooling: spray-mist-quenching with water and pressurized air, quenching only with pressurized air, and air cooling with no active quenching. The setup consists of five nozzle gates with four nozzles each (1 mm nozzle diameter), allowing direct quenching of the complete outer surface area. The water has a temperature of $T_{water} = 20$ °C, is fed in the system at a pressure of $p_{water} = 5$ bar, and is dispersed through compressed air at a pressure of $p_{air} = 4$ bar at the distributor. To investigate the mechanical and microstructural properties of the extruded profiles, tensile tests and microstructural analyses are performed. The tensile tests are carried out in accordance with DIN EN ISO 6892-1, employing a constant strain rate of $\dot{\varphi} = 0.0067$ s^{-1} for testing up to fracture, using a Zwick Z250 universal testing machine. The tensile specimens are laser-cut from the extruded profiles along the extrusion direction and conform to the geometry specified in DIN 50125 – H 12.5 x 50. Five specimens are tested for each parameter set. For the microstructure analysis, the profile cross section is divided into eleven segments due to size constrains. Each segment is subsequently cold mounted, electrolytically Barker-etched and investigated with light microscopy.

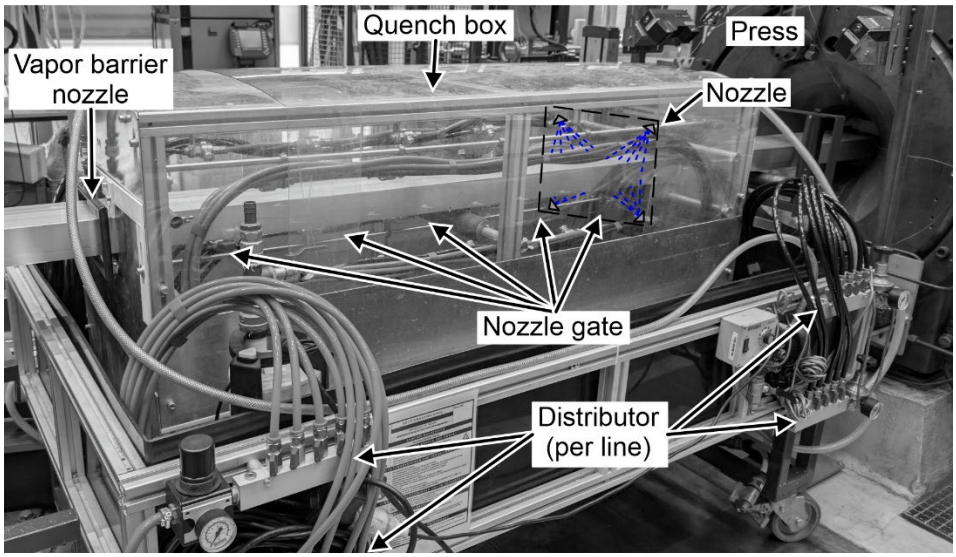

Fig. 3. IUL quench box consisting of five nozzle gates containing of four nozzles each, allowing quenching of the complete outer surface area with pressurized air or water-spray-mist.

Results and Analysis

Die design adaptation. The initial evaluation of the die design is done on a tool design provided by an industrial tool maker according to industrial standards and taking the press and profile dimensions into account. As seen in **Figure 4a,** the design features 7 portholes, with one going through the mandrel to provide sufficient material flow for the middle bridge of the profile. The numerical analysis reveals high stresses exceeding 1000 MPa on the bridges connected to the mandrel, locally reaching up to 1600 MPa. Such stress concentrations would likely result in die fracture and potential tearing of the mandrel. In addition, a maximum mandrel deflection of up to 0.4 mm in the extrusion direction and 0.22 mm in x-direction (**Figure 4b**) of each mandrel is predicted. The primary causes of this behavior can be attributed to the relatively small remaining wall thickness in the outer regions of the tool and the reduced stiffness of the mandrel induced by the central porthole.

To mitigate both the high stress concentrations and the mandrel deflection, several design iterations are performed with the primary objective of increasing the bulk of the bridges and the outer walls of the tool. However, none of these iterations resulted in a satisfactory improvement in tool performance, ultimately rendering this design concept unsuitable for the extrusion of thin-walled, large-scaled profiles. Therefore, a new design developed by OTTO FUCHS KG is introduced (not shown due to confidentially agreement), featuring a more streamlined material flow, a reduction in the number of portholes and an increased mandrel stiffness. The numerical investigation shows a reduction of equivalent stress of 55 % in the localized hot spots and a reduction of the maximum deflection in the extrusion direction of 50 % and in x-direction of up to 77 % (**Figure 4c**). Therefore, this design proves to be usable for extrusion of such thin-walled, large-scale profiles.

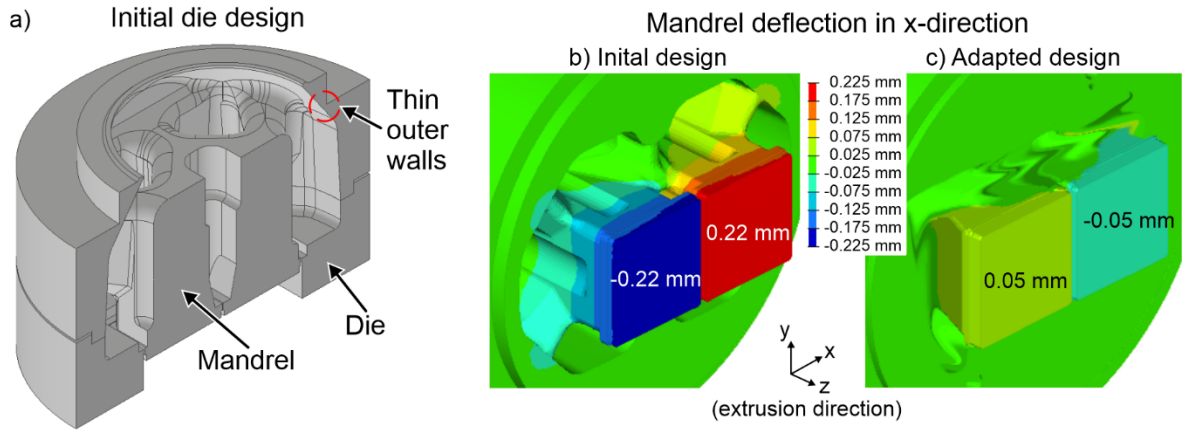

Fig. 4. a) Initial die design and the resulting mandrel deflection in x-direction for b) the initial design and c) the adapted design by OTTO FUCHS KG

Extrusion results. For the validation of the usability of the investigated tool design, several extrusion trials are carried out. Different investigated profile defects, visualizing wrinkling defects at the top and bottom part of the middle web, wrinkling of one or both of the side walls, and a defect-free profile are shown in **Figure 5**. The main reason for these wrinkling defects is a positive relative exit velocity in the center web (**Figure 6a**). As expected for a new tool design, several smaller corrections are necessary to achieve a defect-free cross section. Due to these changes, the outer profile wall thickness needs to be increased to t = 1.15 mm and 1.35 mm for the center web (**Figure 5b** and **c**), to achieve a negative relative exit velocity in the center web to avoid the formation of wrinkles (**Figure 6b**). A weight reduction of 46 % would have been possible with the proposed wall thickness of 1 mm compared to a minimal wall thickness t_{min} = 2 mm found in the literature. However, with the adapted wall thicknesses a final weight reduction of 36 % is achieved with a final *CCD*-to-t_{min} ratio of 138.

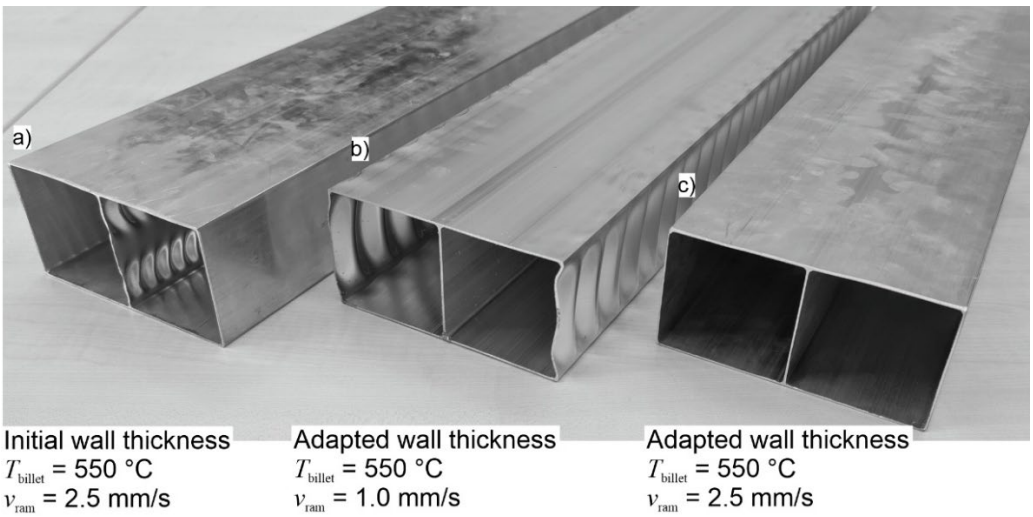

Fig. 5. Extruded profiles showing different defects: a) wrinkling on the center web before wall thickness adjustment, b) wrinkling of the profile side walls after adjustment c) defect-free profile after wall thickness adjustment.

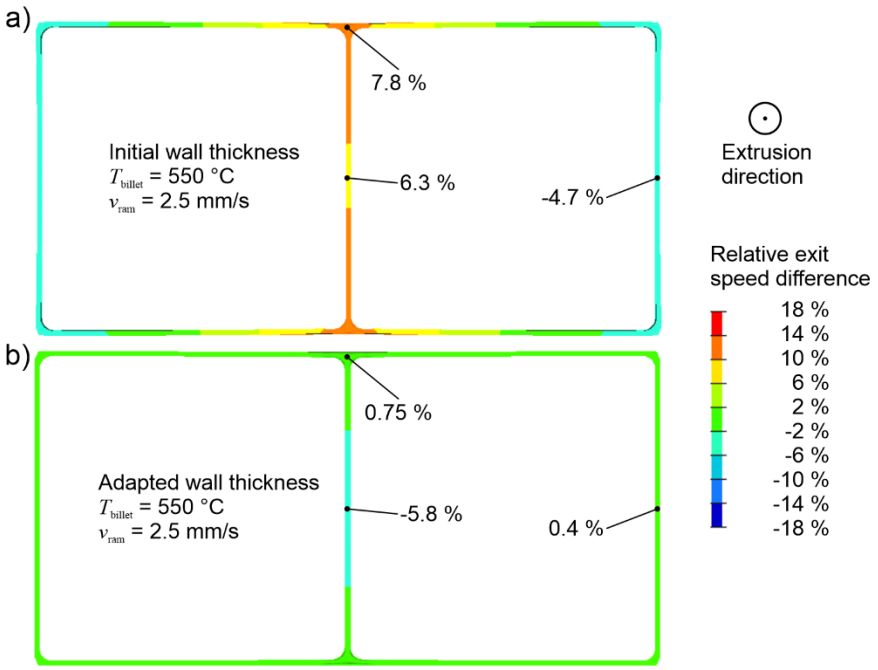

Fig. 6. Numerical calculated relative exit speed difference across the profile cross section correlating to the images of a) **Figure 5a** and b) **Figure 5c**

For the process window, ram speeds between v_{ram} = 2-8 mm/s and billet temperatures between T_{billet} = 530-550 °C are investigated (**Figure 7**). Due to the experimental setup of the used machine, stable processing conditions could be achieved repeatedly with T_{billet} = 550 °C and v_{ram} = 2.5 mm/s. Under these conditions, the heat generated by extrusion and the natural cooling of the tool through the machine frame reach an equilibrium of the profile temperature for each cycle after a brief reheating phase at the beginning of each press cycle (**Figure 7**). The key parameter to achieve defect-free profiles is therefore the surface temperature of the profile at the die exit, which should be between $T_{profile}$ = 490-500 °C. Extrusion at higher or lower profile temperatures $T_{profile}$ due to different billet temperature T_{Billet} or ram speeds v_{ram} results in renewed wrinkling on the side walls of the profile.

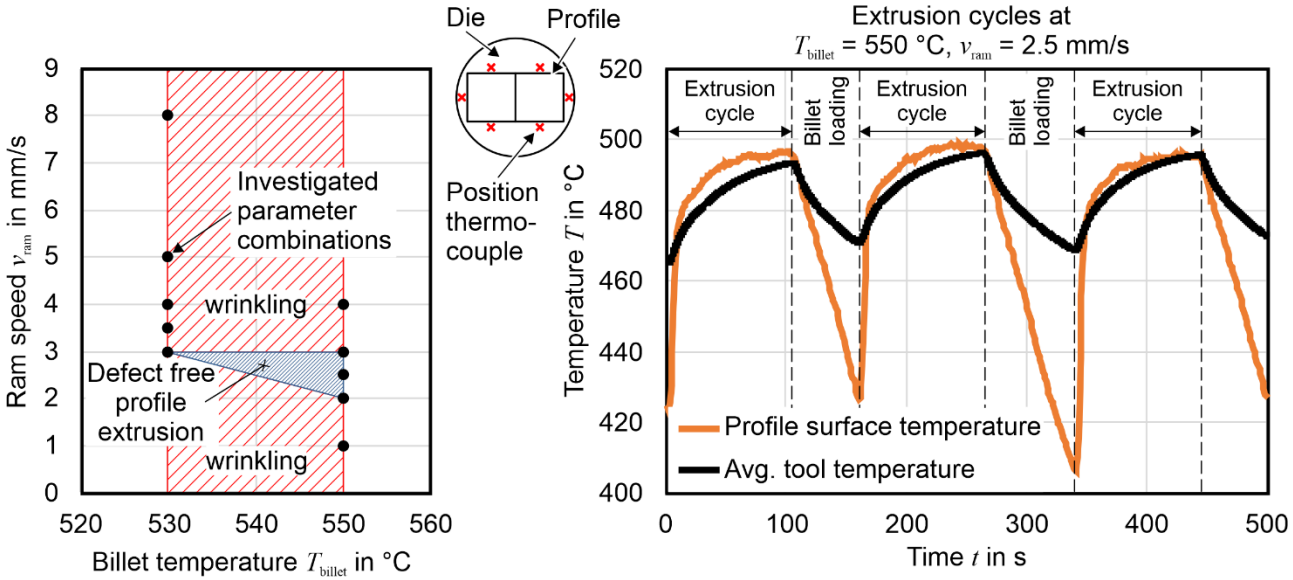

Fig. 7. Process window for extrusion of defect-free profiles and temperature evolution of the average tool temperature and profile surface temperature at the die exit for three extrusion cycles.

Influence of Quenching. For the evaluation of the different quenching methods, the profile deformation caused by quenching is measured by 3D scanning the complete outer surface of the profile using the structured light projection system GOM ATOS. Furthermore, the mechanical properties after quenching are evaluated by tensile tests and the microstructure is investigated of the extruded and quenched profiles. Comparing the measurement of the maximum profile height and width with the tolerances of DIN EN 755-9 (**Figure 8a**) reveal a mostly good fit for the profile height but a in average 0.3 mm to large profile width. This can be attributed to a slight bulging of the side walls. Furthermore, during active quenching (pressurized air or spray-mist) of these thin-walled profiles, the cooling on the top and bottom surfaces is spatially non-uniform, generating steep thermal gradients. These gradients drive different contractions, leading to localized instabilities (wrinkling) that manifest as dimples on the quenched surfaces, which become more pronounced as the cooling-rate increases and a distortion of the cross section of up to 7° can be measured (**Figure 8b**).

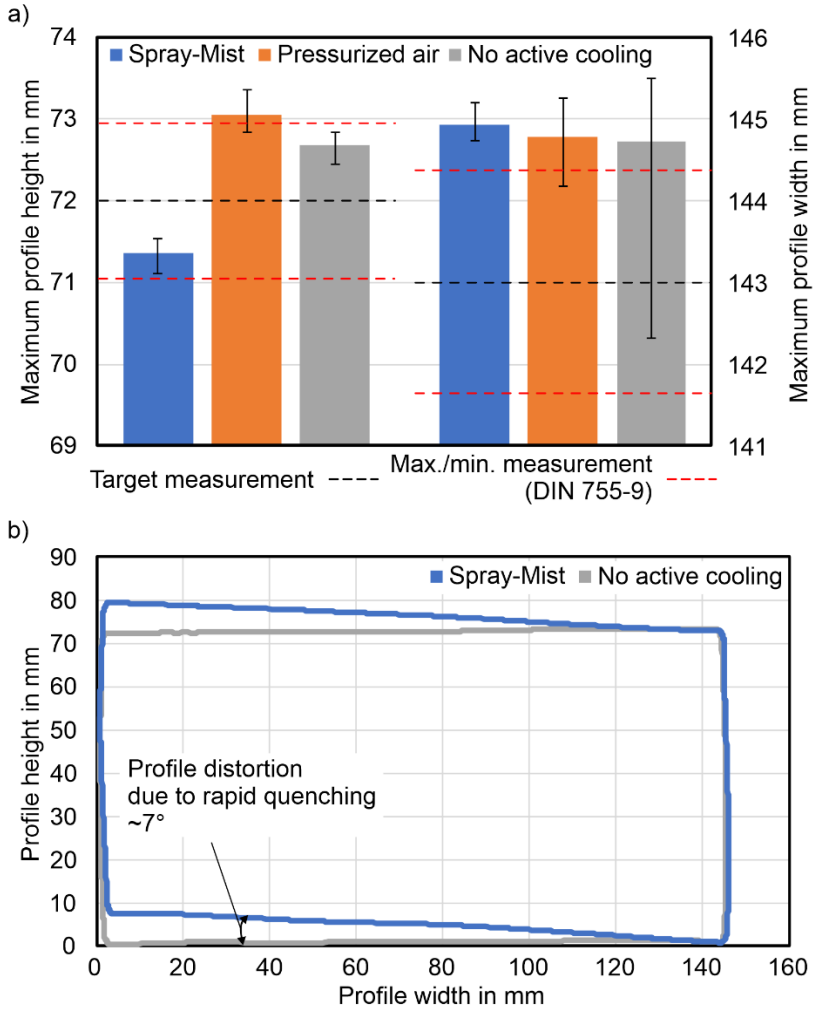

Fig. 8. a) Maximum outer dimension of the extruded and quenched profile in comparison to the tolerances of DIN EN 755-9 and b) cross section distortion due to rapid quenching

Although the distortion behavior of the profiles shows clear differences between the quenching methods, the measured mechanical properties obtained from tensile tests remain essentially unchanged across all conditions (**Figure 9**). The resulting ultimate tensile strength (166-176 MPa) are in agreement with the standard DIN EN 755-2 values for a T4-temper of min. 130 MPa. Furthermore, the deviation between the five tested specimens of each parameter set showed only slight scattering (< 3%). This invariance is most likely attributed to the thin walls and large surface area of the profiles, which enable inherently efficient heat extraction regardless of the applied quenching method. Microstructural examination of the cross sections reveals a narrow-recrystallized edge layer in each wall. Comparing the width of these recrystallized edges in the inner web of the profile only shows a deviation of 4% from 176 µm for no active cooling to 169 µm for spray-mist

quenching. This consistent microstructural morphology further explains the similar mechanical properties and supports the conclusion that the cooling capacity of the thin-walled profiles is already sufficient to achieve the desired metallurgical state. Furthermore, the quenching rates and the profile deformation are also numerically simulated and are in good agreement with the experimental results. These results will be used for further optimization of the quenching process in the future.

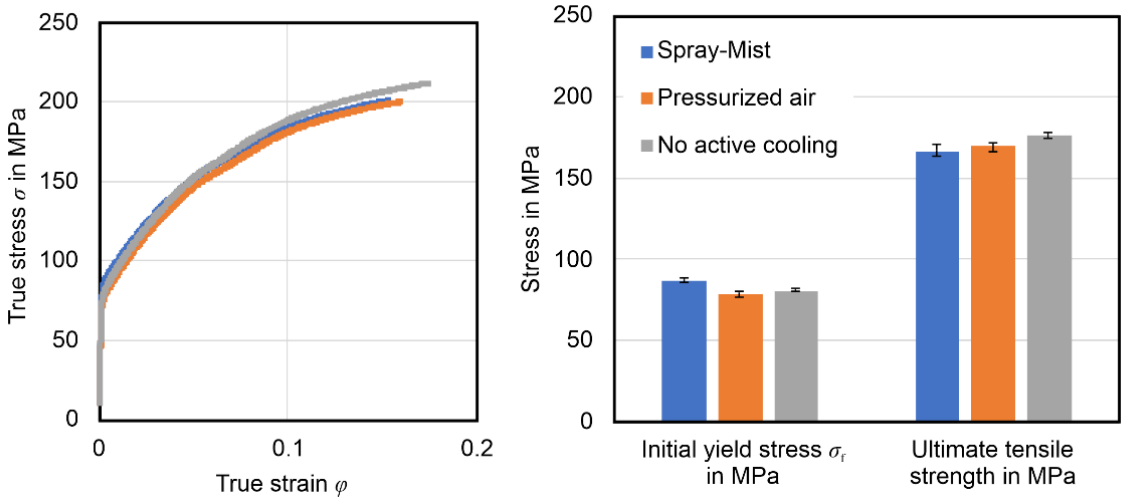

Fig. 9. Average true stress-strain curves for five specimens each and mechanical properties of the extruded profiles using different quenching methods of the laboratory scale.

Scalability of the profile. To investigate size scaling effects, the cross section is geometrically scaled-up by a factor of 2.5, extruding a billet of 344 mm diameter using a 55 MN industrial press. In contrast to the lab-scale extrusion trials, the originally intended wall thickness and *CCD*-to-t_{min} ratio of 160 could be realized (**Figure 10**). This leads to the assumption, that small inhomogeneities of the local profile velocity have a smaller influence while using larger, less wrinkling-prone wall thicknesses, resulting in a more stable process. With the final wall thickness of 2.5 mm, a weight reduction of 38 % is reached compared to a profile with minimal wall thickness t_{min} = 4 mm as typically found in the literature for a *CCD* of 400 mm. The parameter combinations investigated thus far (T_{Billet} up to 530 °C, $v_{Profile}$ up to 9.0 m/min) reveal a similar narrow process window, as for the laboratory scale. However, further extrusion trials are needed as no stationary state is reached, due to the limited amount of extrusion runs under constant process parameters. Therefore, the final process window might also show a higher robustness as seen regarding the wall thickness. While the dimensional tolerances for the laboratory scaled profile are not fully complied with, the upscaled profile show a significant improvement (width tolerance ± 1.6 mm instead of 2.8 mm and height tolerance ± 1.0 mm instead of 1.8 mm). Nevertheless, further investigations, especially of profiles from the steady state, are necessary in order to make final valid statements. The mechanical properties of the upscaled profiles are investigated after a subsequent heat treatment to the T6-temper, to be comparable with the industrial manufacturing process chain of automotive parts. The two different quenching methods result in a final ultimate tensile strength of 266 MPa for pressurized air and 265 MPa for spray-mist quenching and thus meet the requirement of DIN EN 755-2 of at least 215 MPa. This leads to the same assumption, that for the investigated alloy, even the increased wall thickness to 2.5 mm provides sufficient heat extraction through the large surface-area-to-volume ratio.

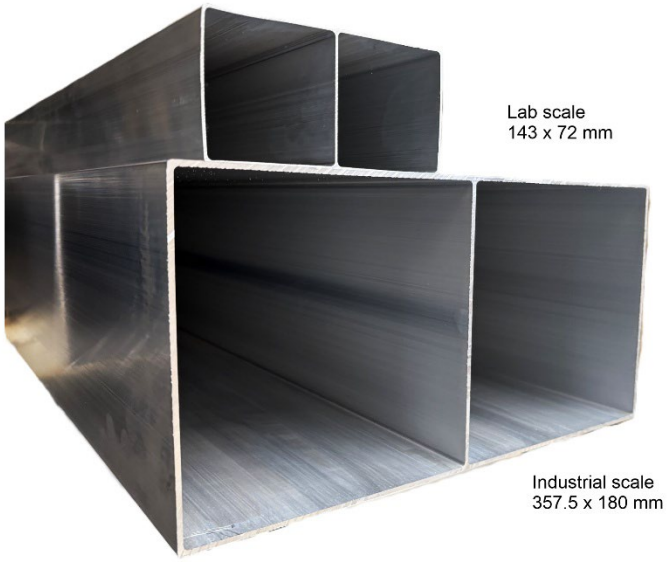

Fig. 20. Comparison of the extruded profiles for both scales

Conclusion

The present investigations demonstrate both the technological feasibility and the current limitations of manufacturing thin-walled, large-scale profiles for modular battery housing applications, achieving a *CCD*-to-t_{min} ratio of 138 and 160 for AA6063. Within the context of sustainable mobility, such lightweight carrier systems offer significant potential to reduce vehicle mass while maintaining structural integrity and enabling efficient thermal management.

Iterative die optimization led to a streamlined design with significantly reduced mandrel deflection, enabling defect-free extrusion under controlled conditions. However, an increase in wall thickness from 1 mm to 1.15 mm in the outer walls and 1.35 mm in the inner web was required to achieve homogeneous material flow within the die. Experimental trials confirmed a narrow process window at T_{billet} = 550 °C and v_{ram} = 2.5 mm/s, resulting in stable surface temperatures at the die exit between $T_{profile}$ = 490-500 °C.

The investigation of different quenching methods showed that active cooling methods (using pressurized air or spray-mist) affect surface deformation, such as wrinkling, but have negligible effects on mechanical properties or microstructure due to efficient heat extraction inherent to the thin-walled, large-scale geometry.

Size scaling investigations using a cross section scaled-up by a factor of 2.5 on an industrial extrusion press revealed similar process stability limits and post-quenching mechanical behavior. The originally intended *CCD*-to-t_{min} ratio of 160 could be realized with the scaled-up profiles and a weight reduction of up to 38 % compared to conventional designs could be achieved. However, further investigations of the process parameters are needed to fully understand the process behavior under stationary conditions.

In summary, the results define key parameters for reliable extrusion and quenching of lightweight modular battery housings, providing a foundation for further optimization towards industrial implementation.

Acknowledgements

This study was funded by the Federal Ministry for Economic Affairs and Climate Action on the basis of a resolution of the German Bundestag (03LB1016C).

References

[1] Wu W, Wang S, Wu W, Chen K, Hong S, Lai Y. A critical review of battery thermal performance and liquid based battery thermal management. Energy Conversion and Management 2019;182(4):262–81. https://doi.org/10.1016/j.enconman.2018.12.051.

[2] Krüger C, Spohr S, Merdivan D, Urban P. Avoiding structural redundancies between the vehicle body and the battery housing based on a functional integration approach. Automot. Engine Technol. 2022;7(3-4):197–208. https://doi.org/10.1007/s41104-022-00106-8.

[3] Kneuper F, Neumann S, Schulze A, Otroshi M, Tekkaya AE, Meschut G. Mechanically Joined Extrusion Profiles for Battery Trays. Automot. Innov. 2024;7(1):182–93. https://doi.org/10.1007/s42154-023-00267-8.

[4] Wehrle R, Baier H. Grid based contour parameterization and optimization of extruded aluminum profiles considering structural and manufacturing aspects. Struct Multidisc Optim 2016;54(4):1031–44. https://doi.org/10.1007/s00158-016-1463-9.

[5] Wan M, Li F, Xia W, Fang X, Jia X. Optimization Design of Porthole Die to Enhance Metal Flow Stability for Thin-Wall, Asymmetric, Unequal-Wall-Thickness (TW-AS-UWT) Aluminum Profile Extrusion. J. of Materi Eng and Perform 2025;191(1):114176. https://doi.org/10.1007/s11665-025-10963-7.

[6] Madura J, Puchlerska S, Balcerzak M, Noga P, Bogusz M, Zasadziński J et al. Development of Low-Weight and High-Strength AA6005A Extrudates Intended for Modern Architecture and Design of Innovative Die for Extrusion Process. Materials (Basel) 2024;17(10). https://doi.org/10.3390/ma17102437.

[7] Murakami T. Welding in multi-billet extrusion. Welding International 1999;13(6):425–9. https://doi.org/10.1080/09507119909447391.

[8] Lv J, Yu J, Shi Z, Li W, Lin J. Feasibility study of a novel multi-container extrusion method for manufacturing wide aluminium profiles with low force. Journal of Manufacturing Processes 2023;85(1980-2015):584–93. https://doi.org/10.1016/j.jmapro.2022.11.055.

[9] Ralls AM, Leong K, Clayton J, Fuelling P, Mercer C, Navarro V et al. The Role of Lithium-Ion Batteries in the Growing Trend of Electric Vehicles. Materials (Basel) 2023;16(17). https://doi.org/10.3390/ma16176063.

[10] QuantumScape Battery I. EV Battery Cell Formats for Lithium Metal. [last visited November 14, 2025]; Available from: https://www.quantumscape.com/blog/ev-battery-cell-formats-for-lithium-metal/.

[11] Ostermann F. Anwendungstechnologie Aluminium. Berlin, Heidelberg: Springer Berlin Heidelberg; 2014.

[12] Zener C, Hollomon JH. Effect of Strain Rate Upon Plastic Flow of Steel. Journal of Applied Physics 1944;15(1):22–32. https://doi.org/10.1063/1.1707363.

[13] Sellars CM, Tegart WJM. Hot Workability. International Metallurgical Reviews 1972;17(1):1–24. https://doi.org/10.1179/imtlr.1972.17.1.1.